

Vanadium Redox Flow Battery: Potentials and Challenges of an Emerging Storage Technology

ABSTRACT

In this paper an overview of Vanadium Redox Flow Battery technologies, architectures, applications and power electronic interfaces is given. These systems show promising features for energy storage in smart grid applications, where the intermittent power produced by renewable sources must meet strict load requests and economical opportunities. This paper reviews the vanadium-based technology for redox flow batteries and highlights its strengths and weaknesses, outlining the research lines that aim at taking it to full commercial success.

1 Introduction

Present electric energy production, exceeding $20 \cdot 10^3$ TWh per year and is growing at a rate of about 3% per year [1–3]. For about four decades scientific forecasts warned that conventional resources cannot stand this increasing demand on the long term [4, 5] and only in recent years central administrations of all industrialized countries have embedded into their development programs several policies for the gradual replacement of carbon-based plants with environmentally-friendly renewable sources. Following these programs, world wind generating capacity has reached 369.6 GW in 2014, with an average growth of 18.4% per year in the last 5 years and the Global Wind Energy Outlook 2014 forecasts a wind capacity over 750 GW by 2020. The global photovoltaic (PV) capacity has grown of 35% in 2013, reaching 177 GW in 2014. The penetration of wind and PV power has exceeded 5% in 2014 and is estimated to increase to more than 25% by 2030 [6–8]. Unfortunately, renewable sources like wind and solar present two major drawbacks with respect to conventional power plants: they are more expensive and intermittent according to time and climatic conditions. While the former drawback can be overcome with the development of advanced devices based on innovative materials and configurations, the latter calls for suitable energy storage (ES) technologies, unless a large oversizing of the grid power and/or a large waste of energy are accepted [9, 10].

At a deeper analysis, the variability of power from renewable sources ranges from the half-day time-scale of sun-light, typical of PV systems [11], down to the min-sec time-scale characterizing wind generators [12], passing through the hourly time-scale of tidal power plants [13]. Grid integration of such intermittent energy sources requires specific care, since conventional grids can become unstable if power penetration from intermittent sources exceeds 20% of the whole generated power without adequate countermeasures [14]. Also under this perspective, the most viable solution consists in complementing energy generation from renewables with ES systems, which enable storing production surplus during some periods and enhancing delivery when demand is higher [15–18]. Stationary energy

storage systems can provide a number of different services, which can be grouped into two main categories, depending on their typical timescales: power quality and energy management. The former refers to charge/discharge cycles on the short timescale (secs–mins) and includes sag compensation, power smoothing, grid stabilization and frequency regulation. The latter concerns charge/discharge cycles on the long timescale (hours) and includes load leveling, load following, power balancing, peak shaving, and time shifting and also contributes towards improving the grid hosting capability [19]. Complementing generation systems with energy storage opens also for interesting economical opportunities. When electric utilities offer policies of hourly pricing, energy storage enables distributors and consumers to reduce their electricity costs. Moreover, large-scale energy storage, by mean of both sparse large plants and dense small/medium size systems, can allow to delay the upgrade of primary power plants, according to a strategy of investment deferral [20]. Depending on all these services, operating times range from fractions of a second to several hours with corresponding response times from milliseconds to several minutes [21,22], while rated powers vary from a few kilowatts to some gigawatts. Economically convenient and technically competitive storage solutions must also have a long calendar life and withstand a large number of charge/discharge cycles.

Storage technologies capable of providing such services are expected to increase dramatically in the near future. A recent authoritative report by the Boston Consulting Group has forecasted investments exceeding US\$10 billion/year on energy storage technologies by 2020 [23]. Presently available ES systems are characterized by different levels of technological development, from mature to emerging, and are suitable for different storage and localization needs. The best performing/promising storage systems for stationary and mobile electric energy applications are: PHES (Pumped Hydro Energy Storage), CAES (Compressed Air Energy Storage), TES (Thermal Energy Storage), FES (Flywheel Energy Storage), SMES (Superconducting Magnetic Energy Storage), EDLC (Electric Double Layer Capacitor), ECES (Electrochemical Energy Storage). Fig. 1 shows how these different technologies are allocated in the power/duration diagram. Among them, at present the first three kinds are suitable for long-time-scale (hours) discharge times, but they cannot cope with fast operations. The first two present tight site constraints, whilst the third is competitive only to defer electric generation of thermo-solar plants. FES, SMES and EDLC have very fast response times, but are effective on the sec-min timescale and are very expensive at present. SMES are in an early development stage, but also the other two require major improvements to become competitive.

In this framework, several surveys indicate that ECES systems are the solution of choice for providing storage services with wide range of discharge times and kilowatt to megawatt power ratings, because of their wide power and energy scalability [23–25]. In fact, they are located in a wide area of the power/duration diagram of Fig. 1 not covered by other storage technologies. These major advantages are complemented with site versatility, very limited

environmental impact, modularity, static structure, and ease of operation. Moreover, they are the only ES technologies exploitable on the large scale for electric mobility. Thus, they are expected to spread widely worldwide in the coming years and substantial funds have been allocated for their future scientific and technological development. Forecasts indicate a growth of the installed power in energy storage technologies to 330 GW and US\$300 billion investments on a global scale by 2030 (250% of present), of which 150 GW (e.g. 45% of the total and 10,000 times the present capacity) in ECES technologies with 50% of the total investment [23].

2 Redox Flow Batteries

Fig. 1 shows that a wide area of the power/duration diagram within the ECES is covered by redox flow batteries (RFBs). The principle behind them is a couple of electrochemical reduction and oxidation reactions occurring in two liquid electrolytes containing metal ions. Both half-cells where the reactions occur are connected to external storage tanks from/to where the solutions are circulated by means of pumps (Fig. 2). This feature provides RFBs with an almost unique advantage on other ECES systems: power and energy ratings are independent. A comparison of the main figures of the more competitive electrochemical energy storage technologies presently available is given in Table 1. VRFB indicates Vanadium redox flow batteries, which are at present the marketed version of RFBs. Cost figures are obtained from contracts recently signed for a multi-technology energy storage facility under construction in Venice (Italy) and show that present commercial VRFBs are already very competitive as compared to other ECES technologies.

In this framework, RFBs are emerging as a promising option for stationary energy storage in electric grids with regard to both power quality and energy management services [9]. RFBs offer several benefits, since they share the aforementioned advantages with the other ECESs (lead-acid, lithium, sodium-sulfur, sodium-nickel-chlorine, nickel-metal, ...) and, furthermore, their power/energy independent sizing allows for long discharge times unachievable with other ECESs, unless they are largely oversized in power. RFBs also present response-time in the order of milliseconds, high overloading for short times, good round-trip efficiency, room temperature operation, low self-discharge, and extremely long charge/discharge cycle life. They are also fully reversible, so that the same device performs both charge and discharge. For several features they are similar to fuel cells (FCs), which also are power/energy independent, but are not reversible, exhibit much lower round-trip efficiency, much lower cycle life and much higher costs.

In RFBs, energy is stored in two electrolytic solutions containing different redox couples. In some cases one solution is substituted with gas or air. The battery heart is a stack made of several cells, each formed of two electrodes separated by an ion-conducting electrolyte (Fig. 3a). The electrodes consist of compartments where the electrolytic solutions are pumped and the half-electrochemical reactions take place during operation. The electrolyte is a polymeric

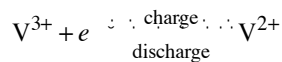
membrane that prevents electrolytic solutions from mixing and allows the passage of ions but not of electrons. The solutions are circulated to/from their external tanks by means of two pumps. Similarly to FCs, this architecture decouples power rating, which depends on the stack size, from stored energy rating, which depends on the tanks volume. The overall stack structure is shown in Fig.3b.

Several chemistries can be used in RFBs, which are under investigation, resorting to both aqueous and non-aqueous solutions: vanadium-vanadium, bromine-polysulphide, zinc-bromine, zinc-cerium, magnesium-vanadium, vanadium-cerium, vanadium-polyhalide, vanadium-bromine, vanadium-oxygen, hydrogen-bromine. Other chemistries, such as quinone-bromide (based on organic quinones) are also investigated, but they appear much more exotic and far from competitive industrial exploitation. Although some promising results have been obtained with other chemistries, the all Vanadium chemistry (V-V) used in the VRFBs is the best developed option so far. It was introduced in the 70s and, though having already reached commercialization, several aspects of its operation remains to be explored and improved [26]. A VRFB exploits the four oxidation states of vanadium, with V(II) (bivalent V^{2+}) and V(III) (trivalent V^{3+}) used at the negative electrode, and V(IV) (tetravalent VO^{2+}) and V(V) (pentavalent VO_2^+) at the positive electrode (the bright colors of the four oxidation states are shown in Fig. 4). These ions are dissolved with concentrations of 1.5–2 M in an aqueous solution of sulfuric acid, with concentration of 2–5 M. The electrochemical half-reactions are:

positive electrode



negative electrode



The ions $2H^+$ (protons) move through the membrane so as to maintain the electrical neutrality of the electrolytes and, in doing so, they close the circulation of electric current, whereas the electrons produce it in the external circuits.

The electrodes where the vanadium solutions are circulated and the half-reactions (1) occur are typically made of highly porous carbon or graphite felts, treated in order to improve their hydrophilicity and to achieve catalytic effects in the half-reactions. Inside the electrodes complex mass transport of the solutions occurs, involving diffusion, convection and migration, according to the Nernst-Planck equation. The ions migrating through the polymer membrane electrolyte are protons H^+ if a cationic membrane is used or anions (e.g. bisulfate HSO_4^-) if an anionic membrane is adopted.

2.1 Cell voltage

Half-reactions (1) produce a cell reversible voltage, i.e. an emf, of $E^0=1.26$ V in standard conditions, namely at $T_0=298.15$ K (25°C) and with balanced molar concentrations c_x in the sulfuric acid solution of the reacting species x . In

real operating conditions, the emf E deviates from E^0 because of the operating temperature T and of the variations of the concentrations c_x , according to the Nernst equation. In turn, the concentrations c_x of the two species in each electrode vary linearly with the state of charge (SOC) in a complementary way, so as to maintaining their sum constant, neglecting side effects. Moreover, E is also affected by the concentration of protons on each faces of the membrane, which depend on the SOC [27]. It can be shown that the cell emf depends on the state of charge s ($s=0$ at full discharge and $s=1$ at full charge) as:

$$E(s) = E^{0'} + \frac{2RT}{F} \ln \frac{s}{1-s} \quad (2)$$

where $E^{0'}=1.37$ V is a corrected standard emf that accounts for proton concentrations and corresponds to $s = 0.5$, R is the gas constant, T the absolute temperature, F the Faraday's constant. Fig. 5a shows how E varies with s according to (2). Neglecting side effects (e.g. species crossover, dealt further on) and with a good approximation, E coincides with the cell open circuit voltage (OCV), so that, based on (2), a simple measure of the OCV can provide the SOC of the solutions [28]. This technique is simple to implement, even if it lacks of precision for intermediate SOC values, due to the local low value of the curve slope and to side effects such as ion crossover. Moreover, it is more precise at higher and lower SOC, where the slope increases and where the control of SOC is more crucial in order to avoid dangerous over- and under-charges.

In both charge and discharge load conditions, the cell voltage v_c differs from the OCV (2), due to voltage drops v_i (>0 in discharge mode, i.e. voltage decrease, and <0 in charge mode, i.e. voltage increase) which depend on the current density j in the cell active area. Such voltage drops have different nature, mainly: electrochemical activation related to the reaction kinetics, species concentration gradients in the electrodes and ohmic losses due to the membrane ionic resistivity (Fig. 5b).

2.2 Cell and stack sizing

The required cell current i_c is achieved by properly sizing the cell cross-sectional area $A = i_c/j_r$. Since the rated current density j_r can reach 0.1–0.15 A/cm² in present commercial devices, cell areas can exceed 50 cm × 50 cm in order to generate currents in the order of 10² A. As a comparison, FCs, which exploit similar cell architecture, have areas at least ten times smaller, thanks to current densities in excess of 1 A/cm². The voltage v_c of a VRFB cell (Fig. 5b) is too low for practical uses, calling for N cells to be connected in series so as to achieve a suitable voltage $v_s = N v_c$, as is common in electrochemical batteries. Properly sizing A and N allows to achieve the rated current and voltage respectively, and thus the rated power. The typical solution for creating the series, inspired by the FC technology,

consists in piling N cells into a stack by interposing a bipolar plate between two next cells, as shown in Fig. 3b. This bipolar plate, usually made of graphite, creates the electrical connection between two cells while separating the positive solution of one cell from the negative solution of the adjacent cell. Holes in the bipolar plates form manifolds inside the stack that provide the parallel distribution and collection of both solutions at all cell electrodes.

3 Side effects and challenges

3.1 Crossover effects

Although VRBs are already commercialized in large systems, up to the 4MW/6MWh plant built by Sumitomo Electric Industries (Japan) for J-Power in 2005, researches are underway for overcoming their present drawbacks and limits with the target of achieving full commercial exploitation [29]. Crossover consists of unwanted diffusive and electro-osmotic transfer of vanadium ions, bisulfate, and water through the membrane. The former effect depends on the concentration gradients between the two electrodes, whereas the latter effect is driven by the ion motion through the membrane. Consequently, not only crossover varies with the different species according to their diffusivity and mobility, but also the two effects occurs with different intensities depending on the SOC and the latter reverses direction in charge and discharge [30, 31]. The overall effect is that charge/discharge cycle after cycle crossover produces a net transfer of vanadium from one compartment to the other, causing a solution imbalance and a reduction of the battery capacity [32]. Moreover, water crossover from one compartment to the other can cause precipitation of vanadium salts, if the limits of solubility are exceeded. For all such reasons, crossover calls for control and corrective measures, the easiest consisting in a periodical redistribution of the solutions between the positive and negative compartments, whereas the more challenging consist in a smart design of the cell membranes.

3.2 Pumping losses and shunt currents

Two more major issues arise in VRFB because they work on liquid electrolytic solutions, which do not pertain to FCs working on gaseous hydrogen and oxygen. Firstly, the higher viscosity of liquid reactants and the larger cell cross-sections imply higher pressure drops and higher pumping powers, which impact on the battery efficiency. Secondly, electric currents flow in both conducting solutions among all homologous electrodes that are at different electrical potentials and fed hydraulically in parallel. These so-called shunt currents depend on the temperature, as usual in electrolytic conductors, and also on the concentrations of the species that contribute to the solution conductivity and vary with the SOC. The joule losses due to shunt currents occur also in stand-by condition reducing the stored energy. Apart from thermodynamics constraints and internal cell voltage drops, pumping losses and shunt currents are the major responsible for the stack losses and consequently affect primarily the system round-trip efficiency. Since reducing the

pumping power calls for short and large piping, whereas reducing the shunt currents calls for long and thin piping, these two issues pose conflicting constraints which can be addressed with advanced designs of stack channels and manifolds, identified by means of CFD combined with numerical optimizers [33].

3.3 Power and energy densities

A major issue of VRFBs is the low power and energy densities, 0.15 W/cm² in the cells, 100 W/kg in the stack, and 25 Wh/kg in the solutions, which imply large stacks and tanks. Such sizes can be acceptable in stationary applications, but they are a drawback with respect to other devices (Li-ion batteries exceed 300W/kg and 200Wh/kg). More compact systems exhibiting higher power and energy densities will resort to non-aqueous electrolytic solutions and/or to improved electrode activity, but also the vanadium aqueous solutions can undergo important progresses [34]. In fact, in small size test cells power densities exceeding 0.55 W/cm² have already been reported [35] and energy densities fourfold higher than present seem at hand. The achievement of these targets stems from new materials for both the porous electrodes and the polymeric membrane. Higher power and energy densities will involve not only smaller devices, but also lower costs and lower inhomogeneity of the physical quantities across the cell area and among the cell forming the stack, which will increase the overall performance.

Present-day commercial VRFBs, with their modest 25–50 Wh/kg, are not suitable for mobility use, but the previous improvements are promising also in this direction. More compact RFB systems, could be competitive for powering electric vehicles, allowing for driving range greater than the one existing in present BEVs (battery electric vehicles) and refueling as fast and easy as gasoline.

4 **Cell and stack modeling**

The careful evaluation of cell and stack performance needs to account for electrochemical, fluid-dynamic electrical and thermal effects. To this aim sets of non-linear equations are used, notably the Butler-Volmer equation to model the electrochemical kinetics and activation overpotentials (i.e. voltage drops in electrical terms) as a function of the current density, the Nernst-Planck equation for mass and ion transport in the electrodes and the Vogel-Tammann-Fulcher equation for ion transport in the membrane. Advanced models of mass-transport in the electrode, such as the Lattice-Boltzmann, can capture the non-linear superdiffusive meso-scale ion behavior in the anisotropic porous media [36]. Based on this set of equations, several multiphysics models have been developed to compute the electric performance of RFB (and notably of VRFB) as function of the varying species concentrations, mass flow rate, and temperature, taking into account the physical-chemical properties of electrodes and membrane. More and more accurate models have been developed which also account for the side effects, such as species crossover through the membrane

and solution imbalance. When the large cells of industrial systems have to be studied, two- and three-dimensional models need to be used in order to account for the gradients of the physical quantities across the cell area. This is a challenging issue because of the prevalently two-dimensional geometries (consisting of strata of thin layers) with aspect ratios exceeding 1000, which imply an extremely critical domain tessellation when approached with conventional finite element techniques, and call for high level simulation package, notably Comsol® and Fluent® and in-house software such as PGD (proper generalized decomposition) [37]. However such models are quite complex and their description goes beyond the scope of this paper. More information can be found in the recent literature [38, 39]. On the other hand, a detailed spatial analysis is not needed when modeling the VRFB interfaces with the power converter for connecting to the grid and with the system supervisor (also referred to as energy management system – EMS –) that is devoted at real-time monitoring and control of the power converter and active components (e.g. pumps and valves) for ensuring the best efficiency in every operating condition. Much simpler models are used in this case, such as reduced-complexity equivalent-circuits which capture the major effects occurring in a VRFB. One example is shown in Fig. 6a, where the controlled voltage source represented the fem E expressed in (2) [40]. The resistances represent the losses due to conduction in the membrane (m), electrochemical activation in the positive and negative electrodes ($a+$, $a-$), and mass flow in the electrodes (d). The capacitors account for the double layer effects at the reaction surfaces inside the electrodes. The four controlled current sources represent the species crossover from one electrode to the other, which are driven by diffusion ($cd+$, $cd-$) and electro-osmotic drag ($ce+$, $ce-$). The controlled current source ($pump$) accounts for the power absorption from the circulating pumps and the equivalent resistor ($shunt$) for the shunt currents in the solutions. Equivalent circuits like these also allow deriving extended and unscented Kalman filters for the estimation of the VRFB SOC [41]. At the simplest level, it can be noted that electrochemical activation losses are much lower than the membrane ohmic losses at full load, while concentration losses are important when the rated current density j_r is exceeded. Thus, in order to determine the electrical requirements for designing the power management system, the resistive voltage drop in the membrane is the major effect to take into account and it can be expressed in per unit area quantities as:

$$v_m = r_m j = (d / \sigma) j \quad (3)$$

where r_m is the specific membrane resistance, d is its thickness, that is kept at a minimum, and σ its conductivity. As usual in electrolytic conductors, σ strongly increases with temperature. A typical value at normal operating temperature (20–30°C) is $r_m = 1.5 \text{ cm}^2$. This value can be increased by 80-100% to account for other loss effects, leading to a prudential equivalent total specific resistance $r_t = 3 \text{ cm}^2$, that allows a simple estimation of the cell voltage as:

$$v_c \approx E(s) - v_t = E(s) - r_t j \quad (4)$$

The corresponding simplified equivalent circuit is shown in Fig. 6b.

5 VRFB management system, supervisor and power electronics

Present literature lacks specific studies dedicated to the optimal management of the VRFB system, including its ancillaries (e.g. pumps, valves), and to power electronics solutions that are able to cope with the unique features of this kind of electrochemical systems. A system supervisor, or management system (MS), that would be able to operate a coordinated control of the electrical, chemical and fluid-dynamic quantities according to the electric input/output power requirements is needed. Even if providing effective operations, actual supervisors of commercial VRFBs are not always fully optimized in order, for instance, to reduce the overall losses and to increase round-trip efficiency. The VRFB MS would need State of Charge (SOC) and State of Health (SOH) on-line data for ensuring an optimized overall system control that allows to meet the power exchange expectations with the grid/load and to increase the reliability and to extend the lifetime of the stack [42], to improve its dynamic performances at the same time.

The SOC on line monitoring allows to trigger the electrolyte rebalancing when it is needed. In VRFBs the cross contamination between the two half-cells is not critical, because both the positive and the negative sides contain vanadium, but unfortunately the crossover phenomena described in Section 3.1 occur. The resulting concentration imbalance appears especially after long-term cycling and it causes a permanent reduction in overall capacity, which is counteracted by electrolyte rebalancing. The literature reports VRFB SOC monitoring methods based on coulomb counting, by requiring an expensive instrumentation or some computationally heavy models, which are not easily and cheaply implementable in commercial VRFB systems. Some other approaches to VRFB SOC evaluation are based on the measurements of the OCV [43] or on Kalman filters [44].

The problem of evaluating the VRFB SOH estimation is instead almost open. It is afforded, although without well-assessed results, in the case of lithium batteries [45] and FCs [46] through Electrochemical Impedance Spectroscopy (EIS), which is now the subject of on-field applications through cheap and reliable electronics [47].

The means for having SOC/SOH on-line data is, as often happens for FCs [47], the switching converter, whose main function is the VRFB interfacing to the external world. Its main features, which make it unique for the VRFB applications, are the wide input voltage operability range, the ability of covering charging and discharging operations, and its bi-directionality. As in the case of lithium batteries and fuel cells, the topological solution consisting in a cascade of two stages, a dc/dc and a dc/ac, allows a high flexibility also for realizing an interface with renewable energy sources, e.g. photovoltaics, which converge to a high voltage bus. The dc/ac converter allows the smart grid connection. A large number of papers dedicated to dc/ac topologies for grid connection of renewable sources is available, e.g. [48],

but unfortunately they often refer to unidirectional and not to isolated solutions. The more challenging issue is the dc/dc topology and control: the main features of the most promising solutions are briefly recalled in the following part of this Section and they have been synthesized in Table 2.

The phase shift Dual Active Bridge (DAB) is a very good candidate for the implementation of the dc/dc VRFB Power Management System PMS [49] (Fig. 7). The adoption of a High Frequency Transformer (HFT) embedded into the dc/dc converter topology allows the galvanic isolation and a high voltage conversion ratio, at the same time. The phase-shift modulation allows changing the current in the filter inductance (L) by acting on the displacement between the square-wave voltages appearing at the output of the left side bridge and at the input of the right side bridge. The sign and the magnitude of the phase-shift angle determine the direction and the amount of the transferred power, respectively. In fact, by referring to the AC side of the active bridges and by assuming that they are operating as a sinusoidal system for the sake of simplicity, it is:

$$P = \frac{V_1 V_2 \sin \theta}{X} \quad (5)$$

where V_1 and V_2 are the amplitude of the first harmonic of the line to line voltages at the two sides of the inductance, its reactance thereof being X , and θ is the angle of displacement between the two sinusoidal waves.

The DAB can also include clamping circuits and resonant tanks for achieving soft-switching operation mode, so that high conversion efficiency and reduced component stresses are achieved (the basic scheme is shown in Fig. 8). In [49] some examples of tanks circuits are reviewed, starting from the classical LC type, also showing that the parasitic parameters can be useful in saving additional components. As pointed out therein, once the switch voltage and current ratings are fixed, the power transmission capability of the DAB is proportional to the number of switches. For instance, two half-bridge topologies, which involve a total of four switches, have twice the power transmission capability of configurations based on single-switch converters (e.g dual-Flyback or dual-Cuk converters), but halved with respect to the DC-DC converters which use two full bridges and require eight switches. For this reason, as well as because of the ripple at the double of the switching frequency it produces, the DAB including two full bridges is preferred, especially for high power applications. The DAB efficiency also depends on how the two bridges are controlled: in [50] an in-depth study of this aspect in the case of a 2-kW automotive application is given.

Especially in high power applications, which is the case of centralized VRFB storage system solutions for smart grids, the relatively low VRFB output voltage requires that the input of the upstream bridge is split so that multi-phase and interleaved configurations are able to manage currents as high as some hundreds of amperes. These solutions also offer the advantage of a reduction of the VRFB current ripple, so that bulky and heavy filtering elements are avoided

and the lifetime of the electrolytic capacitors is increased. The three-phase DAB topology reduces the component stress, but it requires the realization of a three-phase symmetrical transformer having almost identical leakage inductances in each phase [51, 52].

Recently a Current-Fed Resonant Push-Pull Dual Active Bridge (PP-DAB), which adopts a novel modulation strategy allowing the operation in bidirectional mode, has been also presented [53]. It fits with the needs of a VRFB, but its conversion efficiency depends too much on the voltage input variations.

Some interesting features are shown by the solution recently presented in [54], which has some similarities with the PP-DAB, especially because of the wide range of input voltage, low current ripple, soft switching capabilities. The interleaved boost with coupled inductors (IBCI) converter is an isolated topology that is suitable for high step-up applications. In [54] a unidirectional solution is presented and analyzed, both in steady state and by deriving the small signal model that might be used for control purposes. The solution needs to be extended to a bidirectional case and validated at more than a few hundred watts.

As for lithium batteries and FCs, also VRFBs suffer from mismatching problems related to the uneven aging and behavior of the cells connected each other to form the large stack. Although high power VRFBs are actually commercialized for centralized storage solutions, some efforts are done for designing modular solutions that reduce the mismatching impact and allow to scale up the plant easily. An example is the product actually commercialized by Proxima [55] and shown in Fig. 9. VRFB modularity means independent vanadium vessels, but also a low power bidirectional dc/dc converter dedicated to each battery element. From an architectural point of view, the dc/dc converter output terminals can be connected in series or in parallel in order to form the desired array, with distributed control solutions that have been extensively studied in the field of photovoltaic systems [56]. As for dc/dc converter topologies, in this low power (e.g. kW) application the current-fed DAB is the most promising, because it ensures, with respect to the voltage-fed DAB, lower RMS current and zero voltage switching (ZVS) in the whole operating range, thus reaching high efficiency values. Current-fed solutions are preferred as active bridge on the VRFB side, where the input voltage is greatly sensible to the charge/discharge operating mode. The experimental results given in [52], which refer to a three-phase topology, show a conversion efficiency in the range of 92-96%, with the VRFB operating voltage ranging in 24-48 V, the output voltage fixed at 288V, and a transferred power in the range 1-5 kW.

6 Conclusions and future perspectives

Stationary energy storage will be a key feature of future smartgrids and microgrids, since it can provide them with a number of service capabilities ranging from power quality to energy management. In this framework Redox

Flow Batteries are emerging as a very competitive option, due to their unique combination of advantages outlined in this paper. Moreover, they present interesting margins of improvement and the developments pursued in many laboratories of several countries can boost their adoption in the near future.

Two major side effects hampering the efficiency of these devices are shunt currents in the electrolyte solutions and pumping power. New stack topologies are under investigations, in order to reduce these effects with the target of increasing the efficiency by 10% so as to exceed 80% and approach the figures now provided by lithium- and sodium-based batteries. A promising solution relies on the stack topology suggested some years ago, but never investigated nor tested according to the existing literature, that consists in connecting in parallel the cells within a stack [57]. It presents the potentials to minimize shunt currents inside the stack while keeping low the pressure drop and the pumping power. A major contribution to the success of RFBs can come from the industrial electronics area, that is needed to provide advanced high-efficiency power management systems capable of low-voltage high-current bidirectional operations, while coping with the battery voltage variation (Fig. 5). Integrated multi-variable control systems capable of ensuring highly efficient and versatile operations are also pivotal in the market success of next RFBs.

References

- [1] *World Energy Outlook 2013*, International Energy Agency, 2013.
- [2] *2012 Key World Energy Statistics*, International Energy Agency, 2012.
- [3] *Annual Energy Outlook 2013 with Projections to 2040*, U.S. Energy Information Administration, 2013.
- [4] D. H. Meadows, D. L. Meadows, J. Randers, W. W. Behrens III, *The Limits to Growth*, Universe Books, 1972.
- [5] K. S. Deffeyes, *Hubbert's Peak: The Impending World Oil Shortage*, (New Edition), Princeton University Press, 2008.
- [6] European Commission, *Proposal for a Council Decision establishing the Specific Programme Implementing Horizon 2020 - The Framework Programme for Research and Innovation (2014-2020)*, COM(2011) 811 final, 2011/0402 (CNS), 2011.
- [7] S. Chu, A. Majumdar, "Opportunities and challenges for a sustainable energy future," *Nature*, vol. 488, no. 7411, pp. 294-303, Aug. 2012.
- [8] J. M. Barroso's speech at the JTI Launch Event 2014-2020, 09 July 2014 Bruxelles, <https://www.youtube.com/watch?v=Acn4Pry7g6A>, retrieved May 2016.
- [9] P. Alotto, M. Guarnieri, F. Moro: "Redox Flow Batteries for the storage of renewable energy: a review," *Renew. Sust. Energ. Rev.*, vol. 29, pp. 325-335, Jan. 2014.

- [10] S. Vazquez, S. M. Lukic, E. Galvan, L. G. Franquelo, J. M. Carrasco, "Energy Storage Systems for Transport and Grid Applications," *IEEE Trans. Ind. Electron.*, vol. 57, no. 12, pp. 3881-3895, Dec. 2010.
- [11] P. Poggi, G. Notton, M. Muselli, A. Louche, "Stochastic Study of Hourly Total Solar Radiation in Corsica Using A Markov Model," *Int. J. Climatol.*, vol. 20, no. 14, pp. 1843-1860, Nov. 2000.
- [12] A. Sturt, G. Strbac, "Efficient Stochastic Scheduling for Simulation of Wind-Integrated Power Systems," *IEEE Trans. Power Syst.*, vol. 27, no. 1, pp. 323-334, Feb. 2012.
- [13] C.M. Johnstone, D. Pratt, J.A. Clarke, A.D. Grant, "A techno-economic analysis of tidal energy technology," *Renew. Energy*, 49, pp. 101-106, Jan. 2013.
- [14] E.J. Coster, J. M. A. Myrzik, B. Kruimer, and W. L. Kling, "Integration issues of distributed generation in distribution grids," *Proc. IEEE*, vol. 99, no. 1, pp. 28-39, Jan. 2011.
- [15] J. M. Carrasco, L. C. Franquelo, J. T. Bialasiewicz, E. Galván, R. C. Portillo Guisado, M. A. Martín Prats, J. I. León, N. Moreno-Alfonso, "Power-Electronic Systems for the Grid Integration of Renewable Energy Sources: A Survey," *IEEE Trans. Ind. Electron.*, vol. 53, no. 4, pp. 1002-1016, Aug. 2006.
- [16] J. Kondoh, I. Ishii, H. Yamaguchi, A. Murata, K. Otani, K. Sakuta, N. Higuchi, S. Sekine, M. Kamimoto, "Electrical energy storage systems for energy networks," *Energy Conv. Manag.*, vol. 41, n. 17, pp. 1863-1874, Nov. 2000.
- [17] B.P. Roberts, C. Sandberg, "The Role of Energy Storage in Development of Smart Grids," *Proc. IEEE*, vol. 99, no. 6, pp. 1139-1144, June 2011.
- [18] T. Hennessy, *DOE Energy Storage Systems Research Program*, Annual Peer Review, Washington DC, 3 Nov. 2006.
- [19] J. P. Barton, D. G. Infield, "Energy Storage and Its Use with Intermittent Renewable Energy," *IEEE Trans. Energy Convers.*, vol. 19, no. 2, pp. 441-448, June 2004.
- [20] R. Poudineh, T. Jamasb, "Distributed generation, storage, demand response and energy efficiency as alternatives to grid capacity enhancement," *Energy Policy*, vol. 67, pp. 222-231, Apr. 2014.
- [21] S. Sundararagavan, E. Baker, "Evaluating energy storage technologies for wind power integration," *Sol. Energy*, vol. 86, pp. 2707-2717, Sept. 2012.
- [22] A. Zahedi, "Maximizing solar PV energy penetration using energy storage technology," *Renew. Sust. Energ. Rev.*, vol. 15, pp. 866-870, Jan. 2011.
- [23] C. Pieper, H. Rubel, "Revisiting Energy Storage. There is a Business Case," *Boston Consulting Group Report*, Feb. 2011.

- [24] W. F. Pickard, A. Q. Shen, N. J. Hansing, "Parking the power: Strategies and physical limitations for bulk energy storage in supply–demand matching on a grid whose input power is provided by intermittent sources," *Renew. Sust. Energ. Rev.*, vol. 13, pp. 1934–1945, Oct. 2009.
- [25] B. Dunn, H. Kamath, J. Tarascon, "Electrical Energy Storage for the Grid: A Battery of Choices," *Science*, vol. 334, no. 6058, pp. 928-935, Nov. 2011.
- [26] G. L. Soloveichik, "Flow Batteries: Current Status and Trends," *Chem. Rev.*, vol. 115, no. 20, pp. 11533–11558, Sept. 2015.
- [27] K. Knehr, E. Kumbur, "Open circuit voltage of vanadium redox flow batteries: Discrepancy between models and experiments," *Electrochem. Commun.*, vol. 13, no. 4, pp. 342–345, Apr. 2011.
- [28] B. Xiong, J. Zhao, Z. Wei, M. Skyllas-Kazacos, "Extended Kalman filter method for state of charge estimation of vanadium redox flow battery using thermal-dependent electrical model," *J. Power Sources*, vol. 262, pp. 50-61, Sept. 2014.
- [29] A. Parasuraman, T. M. Lim, C. Menictas, M. Skyllas-Kazacos, "Review of material research and development for vanadium redox flow battery applications," *Electrochim. Acta*, vol. 101, pp. 27-40, July 2013.
- [30] S. Won, K. Oh, H. Ju, "Numerical analysis of vanadium crossover effects in all-vanadium redox flow batteries," *Electrochim. Acta*, vol. 177, art. 24218, pp. 310-320. Sept. 2015.
- [31] X.G. Yang, O. Ye, P. Cheng, T.S. Zhao, "Effects of the electric field on ion crossover in vanadium redox flow batteries," *Appl. Energy*, vol. 145, pp. 306-319, May 2015.
- [32] K. Ngamsai, A. Arpornwichanop, "Analysis and measurement of the electrolyte imbalance in a vanadium redox flow battery," *J. Power Sources*, vol. 282, pp. 534-543, May 2015.
- [33] S. König, M.R. Suriyah, T. Leibfried, "Model based examination on influence of stack series connection and pipe diameters on efficiency of vanadium redox flow batteries under consideration of shunt currents," *J. Power Sources*, vol. 281, pp. 272-284, May 2015.
- [34] S. Kim, E. Thomsen, G. Xia, Z. Nie, J. Bao, K. Recknagle, W. Wang, V. Viswanathan, O. Luo, X. Wei, A. Crawford, G. Coffey, G. Maupin, V. Sprenkle, "1 kW/1 kWh advanced vanadium redox flow battery utilizing mixed acid Electrolytes," *J. Power Sources*, vol. 237, pp. 300-309, Sept. 2013.
- [35] D.S. Aaron, Q. Liu, Z. Tang, G.M. Grim, A.B. Papandrew, A. Turhan, T.A. Zawodzinski, M.M. Mench, "Dramatic performance gains in vanadium redox flow batteries through modified cell architecture," *J. Power Sources*, vol. 206, pp. 450-453, May 2012.
- [36] D. Maggiolo, F. Picano, A. Marion, M. Guarneri, "Application of the Lattice-Boltzmann Method for Modeling

- All-Vanadium Redox Flow Batteries”, *Proc. IV International Conference on Particle-based Methods – Fundamentals and Applications - Particle 2015*, Sept. 28-30, 2015, pp. 579-589.
- [37] P. Alotto, M. Guarnieri, F. Moro, A. Stella, “Multi-physic 3D dynamic modelling of polymer membranes with a proper generalized decomposition model reduction approach”, *Electrochim. Acta*, vol. 57, no. 1, pp. 250-256, Dec. 2011.
- [38] Q. Xu, T.S. Zhao, “Fundamental models for flow batteries,” *Progr. Energy Combust. Sci.*, vol. 49 pp. 40-58, Aug. 2015.
- [39] Q. Zheng, X. Li, Y. Cheng, G. Ning, F. Xing, F. Zhang, “Development and perspective in vanadium flow battery modeling,” *Appl. Energy*, vol. 132, pp. 254–266, Nov. 2014.
- [40] X. Qiu, T. A. Nguyen, J. D. Guggenberger, M. L. Crow, A. C. Elmore, “A Field Validated Model of a Vanadium Redox Flow Battery for Microgrids,” *IEEE Trans. Smart Grid*, vol. 5, no. 4, pp. 1592-1601, July 2014.
- [41] B. Xiong, J. Zhao, Z. Wei, M. Skyllas-Kazacos, “Extended Kalman filter method for state of charge estimation of vanadium redox flow battery using thermal-dependent electrical model,” *J. Power Sources*, vol. 262 pp. 50-61, Sept. 2014.
- [42] M. J. Watt-Smith, P. Ridley, R. G. A. Wills, A. A. Shah, F. C. Walsh, “The importance of key operational variables and electrolyte monitoring to the performance of an all vanadium redox flow battery,” *J. Chem. Technol. Biotechnol.*, vol. 88, no. 1, pp. 126-138, Jan. 2013.
- [43] K. Ngamsai, A. Arpornwichanop, “Analysis and measurement of the electrolyte imbalance in a vanadium redox flow battery,” *Journal of Power Sources*, vol. 282, pp. 534-543, May 2015.
- [44] V. Yu, A. Headley, D. Chen, “A Constrained Extended Kalman Filter for State-of-Charge Estimation of a Vanadium Redox Flow Battery with Crossover Effects,” *ASME. J. Dyn. Sys., Meas., Control.*, vol. 136, no. 4, art. 041013.
- [45] P. Gao, C. Zhang, G. Wen, “Equivalent circuit model analysis on electrochemical impedance spectroscopy of lithium metal batteries,” *J. Power Sources*, vol. 294, pp. 67-74, Oct 2015.
- [46] C. de Beer, P. S. Barendse and P. Pillay, “Fuel Cell Condition Monitoring Using Optimized Broadband Impedance Spectroscopy,” *IEEE Trans. Ind. Electron.*, vol. 62, no. 8, pp. 5306-5316, Aug. 2015.
- [47] H2020-JTI-FCH-2014-1 Project HEALTH-CODE “Real operation pem fuel cells HEALTH-state monitoring and diagnosis based on dc-dc Converter embeddeD Eis”, <http://www.pemfc.health-code.eu>
- [48] S. Kouro, J. I. Leon, D. Vinnikov and L. G. Franquelo, 2Grid-Connected Photovoltaic Systems: An Overview of Recent Research and Emerging PV Converter Technology,” *IEEE Ind. Electron. Mag.*, vol. 9, no. 1, pp. 47-61,

March 2015.

- [49] B. Zhao, O. Song, W. Liu, Y. Sun, "Overview of Dual-Active-Bridge Isolated Bidirectional DC-DC Converter for High-Frequency-Link Power-Conversion System," *IEEE Trans. Power Electron.*, vol. 29, no. 8, pp. 4091-4106, Aug. 2014.
- [50] F. Krismer, J. W. Kolar, "Efficiency-Optimized High-Current Dual Active Bridge Converter for Automotive Applications," *IEEE Trans. Ind. Electron.*, vol. 59, no. 7, pp. 2745-2760, July 2012.
- [51] R. W. A. A. De Doncker, D. M. Divan, M. H. Kheraluwala, "A three-phase soft-switched high-power-density DC/DC converter for high-power applications," *IEEE Trans. Ind. App.*, vol. 27, no. 1, pp. 63-73, Jan/Feb 1991.
- [52] Z. Wang; H. Li, "A Soft Switching Three-phase Current-fed Bidirectional DC-DC Converter With High Efficiency Over a Wide Input Voltage Range," *IEEE Trans. Power Electron.*, vol. 27, no. 2, pp. 669-684, Feb. 2012.
- [53] J. Hiltunen, V. Vaisanen, P. Silventoinen, "A bidirectional current-fed resonant push-pull converter for low voltage, high current applications," *Proc. 2013 IEEE Energy Conversion Congress and Exposition (ECCE)*, Article number 6647341, pp. 4770-4774, 15-19 Sept. 2013.
- [54] G. Spiazzi, S. Buso, "Analysis of the Interleaved Isolated Boost Converter with Coupled Inductors," *IEEE Trans. Ind. Electron.*, vol. 62, no. 7, pp. 4481-4491, July 2015.
- [55] <http://www.proxhima.com>
- [56] N. Femia, G. Petrone, G. Spagnuolo, M. Vitelli, *Power Electronics and Control Techniques for Maximum Energy Harvesting in Photovoltaic Systems*, CRC Press, 2013.
- [57] P. M. Spaziante, "Novel design and non-conventional applications for vanadium redox technology," Presented at the *International Redox Flow Battery Forum*, Vienna 15-16 June 2010.

Table 1 – Main data of competing electrochemical storage technologies for stationary services - costs include ancillaries (discharge times are at rated power; cost figures based on 2015 commercial contracts; capex = capital expenditure)

	6 F 6 O 5 : P 4 5 O 6 P I	O G S F 5 4 V 4 B	4 3 I 6	4 3 I 6	4 3 I 6 U
) () 0 1 6 4 9	5 6 F P R : E a 2 9 W a 9 b	R : E 6 7 7 : 4			
&) : & 2 (*)	Ž K N & N I J B K	1 7 P N U	I ? Q	J ? R	P P I R O ? L
Ł & A !	J N I B J K B O	1 7 Q R U	M ? N	L ? O	M N I J I ? I
Ł & A Ł . A ° O	R N B J K I ? N B K	1 7 R I U	M ? N	L ? N N	J O L O L O ? M
fi . A . 3 2	J I I B K I U	1 7 Q P U	M ? I	I ? P J	J K M O L J ? J
l k * 0 * (8 6 @	Q 9 1 0 J (L X 0 0 7 J ħ	1 7 K M U	I ? L	P ? J	W J Q Q I W O K O ? P
# ž ~	K M X J I	1 7 P N U	K I	K ? O N	W O O L W M ? M

Table 2 – Main features of the most promising power converter architectures

/ 6	% O 4 9 : R	1 G I G B	R O 3 F P 7	P G 7 R P T : R 4	. O G P	(G F P	(G F R O G B	E 6 R 9 G 5
E M R F	" 9 & 0 ~ (8 . : * 6 .) , * C ~ ~ D			7 2 9 ' ' * 6) * 2 7 . 8 (. 6 (9 ž 8) 7 9 (*)	1 . , - 4 3 ; * 6	† @ , - (. 6 (9 0 & 8 . 2 ,	3 (9 8 4 6 9 * 8 2 8 7 ž + 8 6 * 7 - . . + 8	
E N F	1 & 0 + A ~ 9 0 0	7 6 . 2) , 0 * * 8 6 . 6) * , * *	4 = & 7 * A 8 < 4	fi : & ž * 0 0 & (/ + 0 3 0 ; . - 8	0 0 & (/ + 0 3 0 ; . - 8	1 & 6) 7 ; . 8 (9 - 0 2 & 2 8 8 8 6 . 4	0 3 4 -) 8 7 ? * 2 4 9 0 0 & 8 . 3 2 @	
E N J F	6 * 7 3 2 & 2 8 8 & 2 /	8 -		fi fi	1 . 2 . 1 . = & 8 3 0 3 2 & , * ! ; . 8 (- . 2 ; . 0 \$ ž 2 8 7 2 8 3 9 0 & 8 . 3 2	" . , - 8 2 4 9 8 (9 6 6 * 2 8	6 + & 6 2 * 5 * 9 ? * 2 (<	
E M R F	/ 7 3 0 & 8 * + 0 < ' & (/) 9 & 0 A	9 & 0 A		7 2 9 ' ' * 6) * 2 7 . 8 (. 6 (9 ž 8) 7 9 (*)	" - * 4 3 * 6	< . ž 7 - & 7 * 2 , 7 - 3 2 8 V ž \$ fi	3 (9 8 4 6 9 * 8 2 8 7 ž + 8 6 * 7 - . . + 8	
E N K F	° 9 6 6 * 2 8 A + * ~) 9 0 0 6 .) ,	8 * + 0 < ' & (/) 9 & 0 A		% # ! @ 4 2 - & 8 7 9 * 6 & 0 0 < 2 , * > (0 & 1 4	1 . , - . + † : * 6 & \$. 7 4 . / * / 2 4 9 8 # 3 0 8 & ; * 6 8 6 & 2 7 + 3 6 (1 . * 6 (9 . 8 6 < 8 9 6 2 6 & 8 * (3 3 1 1 * 2) *)	4 - & 7 * A 7 - . . + 8 @ >) 9 8 < A (< (0 * (3 0 8 6 3 0 > * (9 6 6 * 2 8 A 1 3) * (3 2 8 6 3 0		

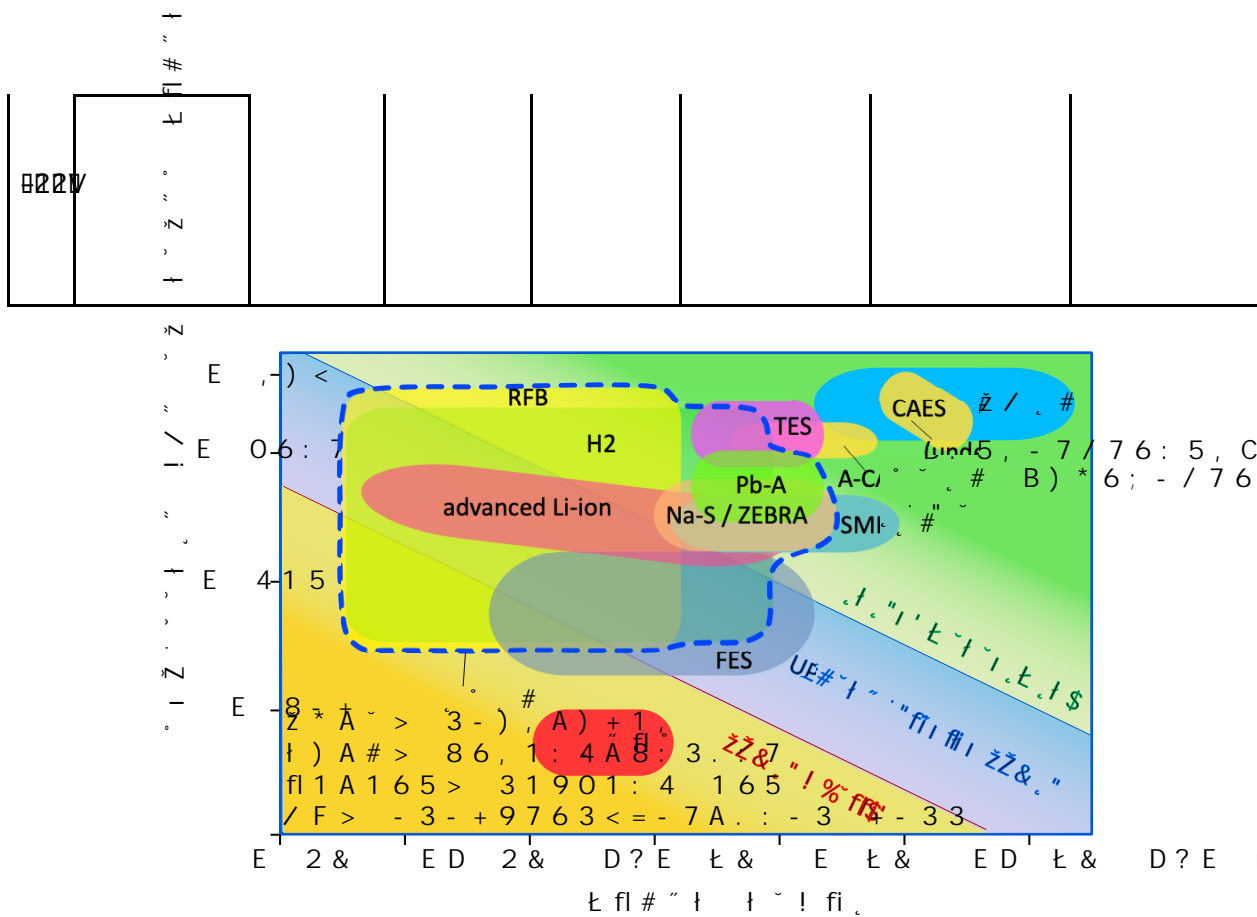


Fig. 1 – Power-duration diagram of existing energy storage systems. The blue dotted line encircles ECES (electrochemical energy storages)

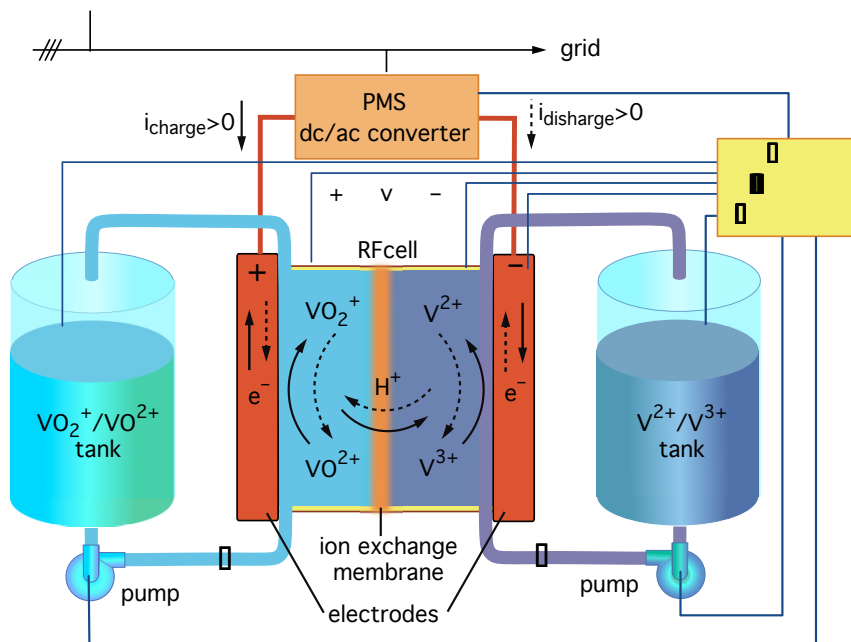


Fig. 2 - Scheme of a VRFB - The liquid electrolytes are actively cycled between the cells and two tanks by means of two pumps.

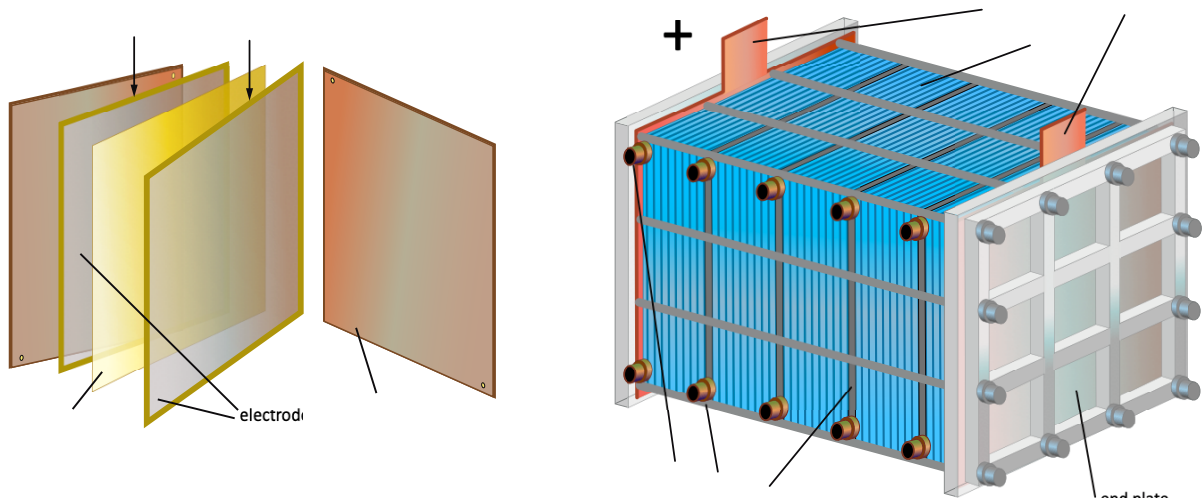


Fig. 3 – a) Exploded view of the structure of a RFB cell, made of a central polymer electrolyte membrane, two porous electrodes, and two graphite current collectors. b) Sketch of a typical VRFB stack, made of N cells connected in direct series through bipolar plates.

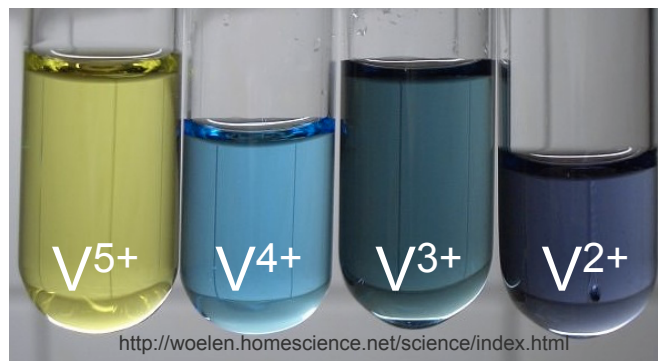


Fig. 4 - Vanadium exhibits the notable feature of presenting four oxidation states, characterized by different brilliant colors (Courtesy of homescience.net).

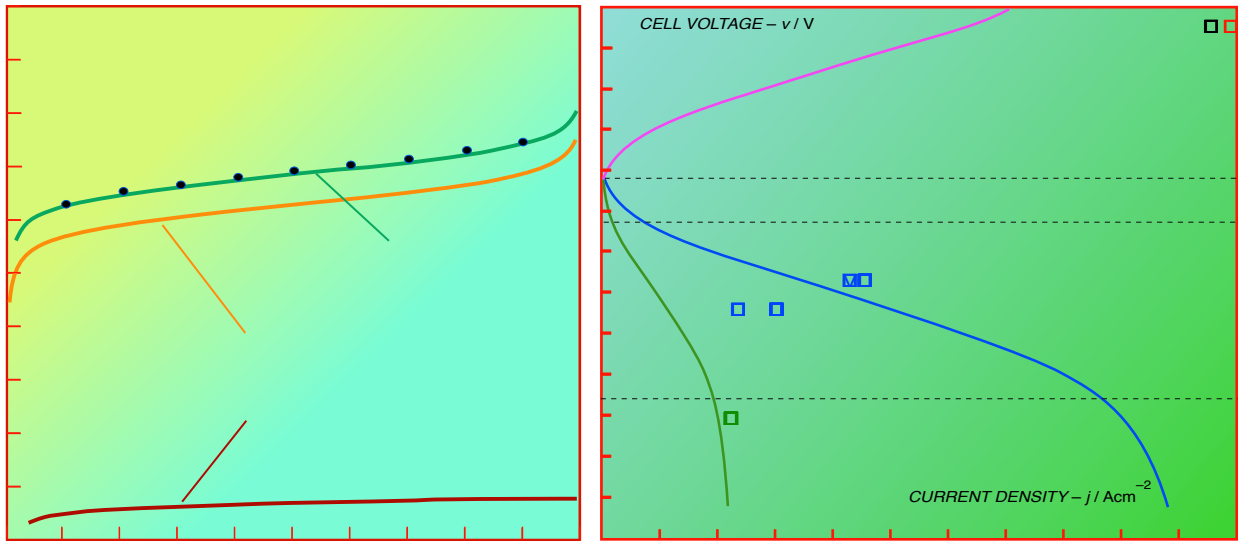


Fig. 5 - VRFB-cell voltage: a) emf, that is basically the open circuit voltage (OCV), as a function of the SOC (state of charge) with experimental data from [28], b) polarization curve, e.g. load voltage as a function of the cell current density at SOC=100%

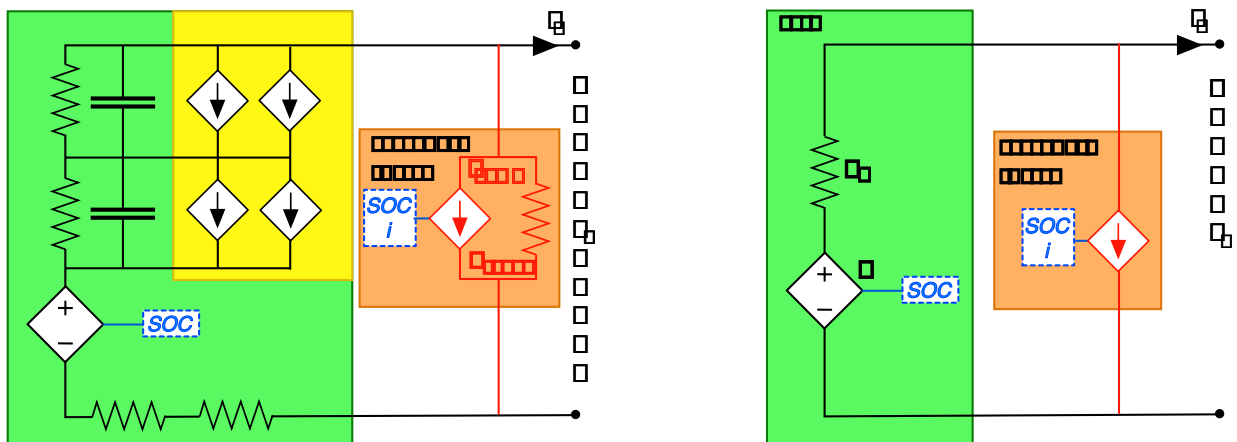


Fig. 6 – Equivalent circuitsof a VRFB cell. a) detailed: E is the SOC-dependent emf; R_{a+} , R_{a-} , R_m , and R_d represent the internal losses due to electrochemical activation in the positive and negative electrodes, conduction in the membrane, and mass flow in the electrodes, respectively. C_{dl+} and C_{dl-} account for the double layer electrostatic effects at the reaction surfaces. I_{cd+} , I_{cd-} , I_{ce+} , I_{ce-} represent species crossover driven by diffusion and electro-osmotic drag, respectively. I_{pump} accounts for the pumping power needed for circulating the solutions, that depends on both ccell current I and SOC, and R_{shunt} accounts for the shunt currents. b) simplified: R_t is a Thévenin equivalent resistor accounting for all cell internal losses whereas I_{loss} accounts for all external losses (shunt currents and pumping)

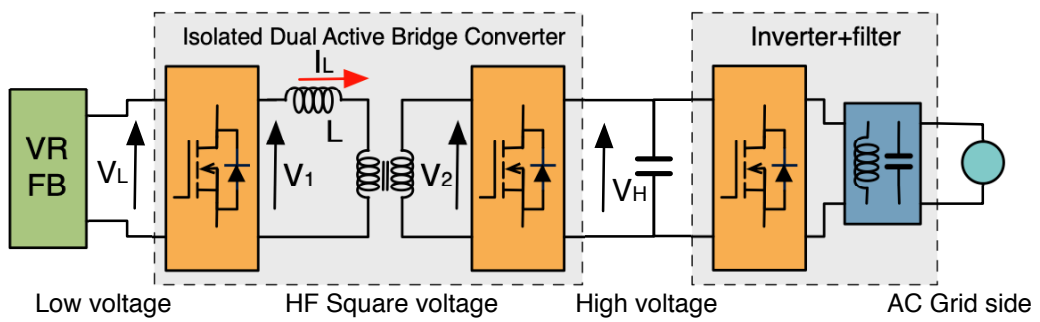


Fig. 7 – Phase shift Dual Active Bridge (DAB) [49]

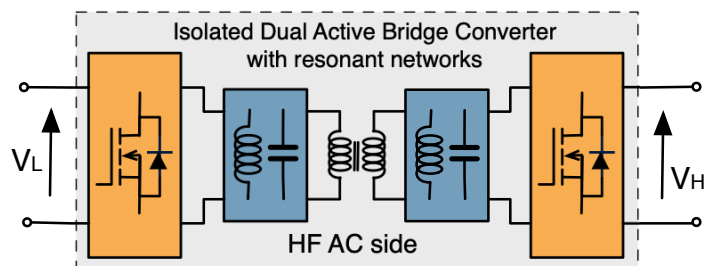


Fig. 8 – Phase shift Dual Active Bridge with resonant tanks



Fig. 9 – Proxima VR 24-C6 modular VRFB. Each unit is rated 4 kW, 64-40 V, 24 kWh (courtesy of Proxima)